Effect of pore water saturation on the supercritical carbonation of cementitious materials

Hao Bao[1, 3], Ruyu Wang[1], Yahui Yang[2,*], Qing Wang[1], Gang Xu[1,*], Mohamed Saafi[3], and Jianqiao Ye[3]

1 College of Civil Engineering & Architecture, China Three Gorges University, Yichang, China

2 College of Hydraulic & Environmental Engineering, China Three Gorges University, Yichang, China

3 School of Engineering, Lancaster University, Lancaster LA1 4YR, UK

* Correspondence author: yangyahuiconcrete@163.com (Y. Yang), postxg@163.com (G. Xu)

Abstract: The optimization of pore water saturation is essential to improve the supercritical carbonation efficiency of cementitious materials. In this study, a control method was developed to adjust the pore water saturation of cementitious materials to predetermined target values, thereby achieving a uniform distribution of pore water within the specimens. Based on this approach, a systematic supercritical carbonation test was conducted, the effects of pore water saturation and water-cement ratio on carbonation efficiency was researched by measuring carbonation depth, which reaches its maximum at a pore water saturation of 0.50. The effect of pore water saturation on the supercritical carbonation depth was clarified. Additionally, a novel method was proposed to determine the $Ca(OH)_2$ and C-S-H contents of cementitious materials before carbonation using inverse derivation from the differences in thermogravimetric analysis (TGA) results. Furthermore, microscopic techniques, including scanning electron microscopy (SEM), were employed to investigate the mechanisms of supercritical carbonation in cementitious materials under different pore water saturation levels. The influence of pore water saturation on the carbonation process was thereby elucidated.

Keywords: Cementitious materials; Supercritical carbonation; Pore water saturation; Water to cement ratio; C-S-H carbonation; Carbonation depth.

1. Introduction

Carbonation is a fundamental chemical process that significantly influences the durability and performance of cementitious materials [1-3]. It occurs when CO_2 penetrates the pore structure and reacts with hydration products, particularly $Ca(OH)_2$ and C-S-H, to form calcium carbonate ($CaCO_3$) [4,5]. Under conventional atmospheric conditions, carbonation is a slow process, governed primarily by the diffusion of CO_2 through the pore network [6,7]. This reaction leads to pH reduction, which can impact the passivation layer protecting embedded steel reinforcements, thereby increasing the risk of corrosion [8,9]. While traditional studies have focused on ambient carbonation, the development of supercritical carbonation

techniques has introduced new possibilities for enhancing the efficiency of the process [7], accelerating CO_2 uptake [10,11], and improving material properties [12-16]. Supercritical carbonation refers to the exposure of cementitious materials to CO_2 in its supercritical state, where it exhibits both gas-like diffusivity and liquid-like solubility. This state, typically achieved at temperatures above 31.1°C and pressures exceeding 7.38 MPa, enables rapid penetration of CO_2 into the cement matrix, enhancing the reaction kinetics [17]. The process has garnered increasing interest due to its potential applications in carbon sequestration and the accelerated curing of cement-based composites. However, despite the advantages of supercritical carbonation, its efficiency is strongly influenced by the internal moisture conditions of the material, particularly the degree of pore water saturation [18]. Since water acts as both a transport medium for dissolved CO_2 and a potential barrier to gas-phase diffusion, understanding its role is crucial in optimizing supercritical carbonation processes for enhanced performance and sustainability.

Pore water saturation plays a complex and dual role in the carbonation of cementitious materials. On one hand, a certain amount of water is necessary to facilitate the dissolution of CO_2, which leads to the formation of carbonic acid (H_2CO_3) [19]. This weak acid further reacts with $Ca(OH)_2$ and other alkaline components to form stable carbonate phases [20]. Additionally, in partially saturated materials, capillary condensation enhances the mobility of ionic species, promoting the diffusion-controlled reaction process. On the other hand, excessive water content can limit the ingress of CO_2 by filling the pore structure, thus acting as a diffusion barrier [21]. This competition between diffusion and dissolution processes creates an optimal range of moisture conditions that maximize carbonation efficiency. Several studies have investigated the impact of relative humidity [22-25] and water to cement (w/c) ratio [26-29] on conventional carbonation. It is well established that carbonation rates are highest at intermediate RH levels (typically around 50-70%), where there is sufficient moisture for CO_2 dissolution but not enough to fully block gas-phase diffusion. However, under supercritical conditions, CO_2 behaves differently, exhibiting higher solubility and penetration capacity than in its gaseous state [30,31]. This altered transport mechanism necessitates a reevaluation of the traditional moisture-carbonation relationship to determine how pore water saturation affects supercritical carbonation kinetics. Understanding this relationship is particularly important for engineered carbonation processes aimed at enhancing material properties and increasing carbon storage efficiency.

The application of supercritical carbonation has been explored for various engineering purposes, particularly in the improvement of mechanical properties [32,33], durability [34,35], and sustainability [17,36]

of cement-based materials. One of the key benefits of this process is the formation of dense and well-crystallized $CaCO_3$ phases, which can significantly refine the microstructure of cementitious composites [37,38]. This densification reduces porosity, enhances compressive strength, and improves resistance to water ingress, thereby extending the service life of structures. Additionally, the rapid reaction kinetics associated with supercritical conditions allow for accelerated curing processes, which can be beneficial in precast concrete production. Another significant advantage of supercritical carbonation is its potential role in carbon sequestration [39,40]. The cement industry is one of the largest contributors to anthropogenic CO_2 emissions [41], primarily due to the decarbonation of limestone during clinker production. By utilizing supercritical CO_2 to accelerate carbonation, it is possible to convert a portion of these emissions into stable carbonate phases within the material itself, effectively reducing the carbon footprint of cement-based construction [39]. However, the efficiency of this sequestration approach is heavily dependent on the pore structure and moisture content of the material. If the material is too dry, CO_2 diffusion is facilitated, but reaction rates may be limited by the lack of aqueous phase. Conversely, if the material is oversaturated, carbonation is impeded due to restricted gas-phase transport. Therefore, optimizing pore water saturation is essential for maximizing both mechanical enhancement and carbon storage potential.

Given the intricate interplay between pore water saturation and supercritical carbonation, a systematic investigation is urgently required to determine the optimal moisture conditions that maximize reaction efficiency. This study aims to examine the influence of varying degrees of pore water saturation on the supercritical carbonation of cementitious materials. By precisely regulating the uniform distribution of pore water saturation, this research analyzes key parameters such as carbonation depth, phase transitions, and microstructural changes before and after supercritical carbonation. Furthermore, a quantitative relationship between saturation degree and carbonation depth is established. Additionally, a novel calculation method is proposed to determine the content of C-S-H and $Ca(OH)_2$ in cementitious materials prior to carbonation based on the supercritical carbonation approach. To elucidate the underlying mechanisms governing the impact of pore water saturation on the supercritical carbonation process, advanced characterization techniques, including TGA and SEM, will be employed.

2. Materials and experimental program

2.1. Raw materials and mix proportion design

The selected fine aggregate was river sand, with a fineness modulus of 2.9 (medium sand) and an apparent density of 2650 kg/m^3. For the coarse aggregate, 5-10 mm pebbles were used instead of crushed stone to prevent the $CaCO_3$ in crushed stone from affecting $CaCO_3$ content measurements in the carbonation test. The pebbles have an apparent density of 2650 kg/m^3 and a crushing index of 9%. Portland cement (P·O 42.5 N) was obtained from Hubei Yichang Yihua Co., Ltd. and used in this study. Its density was measured as 3.1 g/cm^3. Ordinary Portland cements (OPC) have a simple and homogeneous chemical composition, ensuring greater experimental accuracy and reproducibility compared to systems containing supplementary cementitious materials (SCMs), which exhibit considerable compositional variability and require complex optimization. Consequently, this study focuses exclusively on the supercritical carbonation behavior of OPC. The main chemical composition is detailed in Table 1.

Table 1 Main chemical composition of cement.

Components	SiO_2	Fe_2O_3	Al_2O_3	CaO	K_2O	SO_3	Loss of ignition
By mass (%)	19.27	3.36	3.72	67.11	1.24	4.33	0.97

To investigate the effects of pore water saturation and water-cement ratio on the supercritical carbonation of cement-based materials, cement mortar and concrete specimens were designed for the study. The carbonation depth of cementitious materials was observed to be greater under an ambient relative humidity of 0.50 [22, 23]. Accordingly, the pore water saturation levels were controlled at 0.40, 0.50, 0.60, and 0.70, respectively. Simultaneously, the water-to-cement ratios were maintained at 0.4, 0.5, and 0.6. The specific methodologies employed to control pore water saturation are described in detail in Section 2.3. Table 2 shows the mix proportion of cement mortar and concrete.

Table 2 Mix proportion of cement mortar and concrete.

	Water-cement ratio	Cement (kg/m^3)	Fine aggregate (kg/m^3)	Coarse aggregate (kg/m^3)	Water (kg/m^3)
Cement mortar	0.4	600	1261	-	240
	0.5		1227	-	300
	0.6		1129	-	360
Concrete	0.4	375	769	1106	150
	0.5		772	1065	188
	0.6		774	1026	225

2.2. Preparation of cement-based materials

To minimize the effect of material non-homogeneity on the experimental results, three specimens were prepared for each set of conditions. The high-pressure chamber (SLD20) features an inner diameter of approximately 220 mm and a depth of around 480 mm. The chamber has a nominal volume of 20 liters. Due

to the chamber's limited capacity, the specimens were arranged in three layers, with two cubic specimens (each with a side length of 70.7 mm) positioned in each layer. The design temperature and pressure are 200 °C and 12.5 MPa, respectively.

Prior to casting the cementitious specimens, the LF-50305 water-based release agent was evenly applied to the inner surface of the test molds, which were manufactured by Wenzhou Nuofu Building Materials Co., Ltd. The release agent appeared as a milky white liquid, with a film-forming time of approximately 30 minutes. The use of this release agent had negligible influence on the results of the carbonation tests [42,43]. The specimens were cast according to the mix proportion of cement mortar and concrete in Table 2, and the cast and molded cement mortar and concrete specimens were placed in a standard curing box (YH-90B type) for curing to control the curing temperature of 20℃, relative humidity ≥95%, and the mold was removed after 24h of curing. During the curing process of cementitious materials, their internal pores contain saturated $Ca(OH)_2$ solution because of hydration reaction [18], in order to control the initial internal pore water saturation of 100%, and at the same time to ensure that the relative humidity of the subsequent curing is still ≥95%, and to prevent Ca^{2+} leaching inside the cementitious material, the specimens after the removal of molds were placed into the saturated $Ca(OH)_2$ aqueous solution at (20±2)℃ (0.0118 mol/L) for 28 d to realize the control of the initial pore water saturation of the specimens.

2.3. Method for controlling uniform distribution of pore water saturation in cement-based materials

Cement-based materials, as heterogeneous materials, exhibit uneven pore water distribution [44], which can influence the carbonation process [45] and thus affect the results. To accurately study the impact of pore water saturation on the carbonation performance of cement-based materials, precise evaluation of pore water saturation is essential. However, no standardized method currently exists for testing and controlling pore water saturation in these materials. To enable precise control of pore water saturation and clarify its influence on the supercritical carbonation process, methods were proposed to manage uniform distributions of pore water saturation in cement-based materials.

In order to control the different pore water saturation inside the cement-based material, the specimens cured for 28 days were removed from the saturated $Ca(OH)_2$ solution. The control of the uniform distribution of pore water saturation in specimens can be summarized as follows:

(1) The surface water was removed, and the specimen's mass was measured using an FD-C60002 electronic balance with an accuracy of 0.01 g to determine the average mass (m_s) of the specimen in a fully saturated pore water condition.

(2) To accurately measure the pore water saturation at different drying times, the samples were placed in an oven (DZF-6050) with a drying temperature of 60℃, the specimens were removed and the mass was measured at the following time intervals: 8h, 16h, 24h, 48h, 72h, ..., 192h. The corresponding mass (m_i) of each specimen was recorded. When the specimen reached a constant mass, the mass at this point was noted as m_0, indicating the mass of dried specimens.

(3) The pore water saturation (S_i) of the specimen at each drying time is calculated using formula (1).

$$S_i = \frac{m_i - m_0}{m_s - m_0} \tag{1}$$

where i is the drying time. m_i is the mass of the specimen at each drying time (g). m_0 is the mass of the specimen when it is dried to a constant mass (g). m_s is the mass of the specimen when it is fully saturated with pore water (g).

(4) After being processed according to step (3), the specimen achieves control over its average internal pore water saturation. However, the pore water distribution is clearly non-uniform, Based on the pore water saturation control method proposed by DO McPolin et al. [46], the specimens with non-uniform distribution of pore water saturation were placed in a constant temperature and humidity curing box (YH-90B) with corresponding relative humidity. The temperature and humidity control accuracy of the curing box has a temperature control range of 5-50 °C with an accuracy of ±1.0 °C, and a humidity control range of 1%-100% with an accuracy of ±1.5%, respectively. The temperature was set to 20℃, and the wet steady state pretreatment was carried out for 30 days, so that the pore water inside the specimens could be evenly distributed [22,47,48].

(5) Specimens that had completed the control of uniform distribution of internal pore water saturation were removed from the curing box for subsequent supercritical carbonation tests.

The schematic illustration of uniform control of pore water saturation of specimens is shown in Fig. 1.

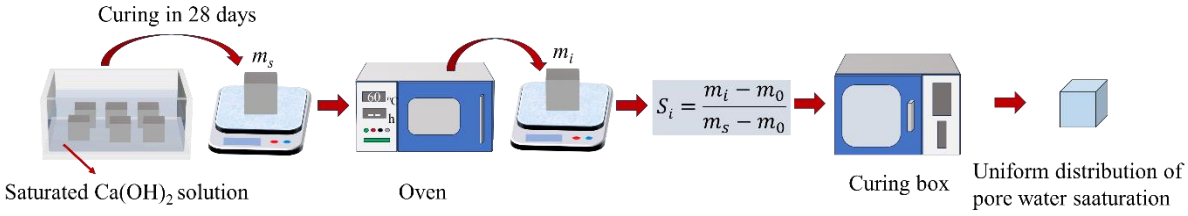

Fig. 1. Schematic illustration of uniform control of pore water saturation of specimen.

To investigate the influence of pore water saturation on the outcomes of supercritical carbonation in cement-based materials, as well as to more clearly observe the carbonation depth and degree after the

completion of the tests, this study sets different pore water saturation levels (0.40, 0.50, 0.60, 0.70) under a fixed water to cement ratio of 0.6. Additionally, to explore the effect of the water to cement ratio on supercritical carbonation results, experiments were conducted with a fixed pore water saturation of 0.50 and water to cement ratios of 0.4, 0.5, and 0.6. For each condition, the specimens were treated with uniform distribution of pore water saturation. The experimental design is shown in Table 3. According to the conditions in Table 3, six specimens were cast for each test to conduct supercritical carbonation experiments.

Table 3. Specimens design.

Groups	Water-cement ratio	Pore water saturation
M-R0.4-S0.50	0.4	0.50
M-R0.5-S0.50	0.5	0.50
M-R0.6-S0.40	0.6	0.40
M-R0.6-S0.50		0.50
M-R0.6-S0.60		0.60
M-R0.6-S0.70		0.70
C-R0.4-S0.50	0.4	0.50
C-R0.5-S0.50	0.5	0.50
C-R0.6-S0.40	0.6	0.40
C-R0.6-S0.50		0.50
C-R0.6-S0.60		0.60
C-R0.6-S0.70		0.70

Remarks: M(C)-R0.4-S0.50 denotes the cement mortar (concrete) specimens with the water to cement ratio of 0.4 and pore water saturation of 0.50.

2.4. Test method for supercritical carbonation of cement-based materials

To study the effect of pore water saturation and water-cement ratio on the supercritical carbonation process of cement-based materials, the supercritical carbonation equipment of cement-based materials was assembled according to the schematic diagram of supercritical carbonation system shown in Fig. 2. The design temperature of the reaction chamber (SLD20) is 200℃ and the design pressure is 12.5MPa. The CO_2 pressurization system consists of a gas booster pump (DGS-DGA25-H), an air compressor (HR230331A), and a filter (015QSP), which operate in combination. The driving pressure of the gas booster pump ranges from 2 to 8 bar. The air compressor operates at a pressure of 0.8 MPa. The CO_2 in the test was from Yichang Dexin Practical Gas Co., Ltd., with purity ≥99.5%.

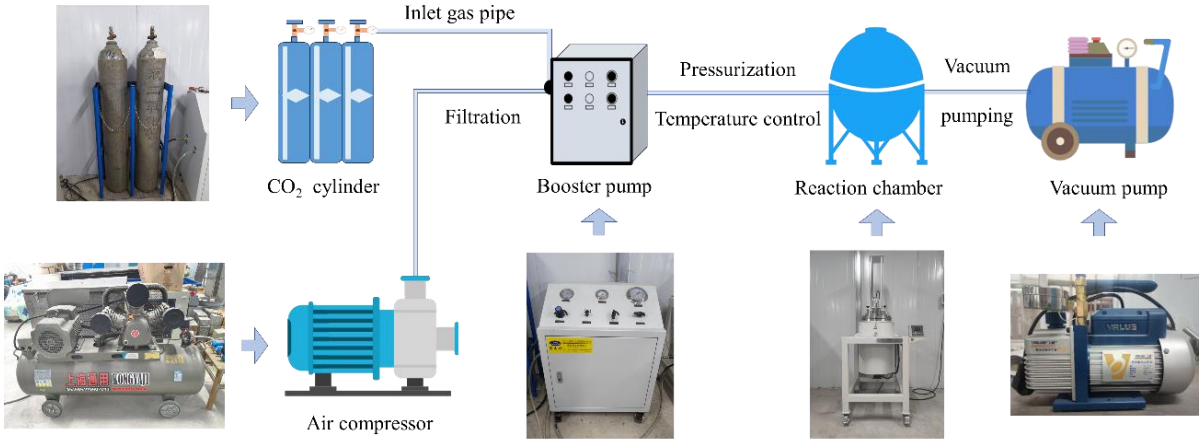

Fig. 2. Diagram of supercritical carbonation system.

(1) The specimens that have completed pore water saturation control placed on the bracket, with three specimens per layer, arranged in three layers for a total of nine specimens. Then, the bracket was placed into the reaction chamber to conduct the supercritical carbonation test.

(2) The reaction chamber cover was closed and the high-strength nut was tightened using a torque wrench. The CO_2 cylinder, pressurization system, and reaction chamber were connected with a high-pressure hose. The inlet valve of reaction chamber was closed, the exhaust valve was opened, and a vacuum pump was connected to one end of the exhaust valve. The vacuum pump was turned on and the reaction chamber was evacuated until the vacuum gauge indicates -0.1 MPa. Then, both the exhaust valve and the vacuum pump were closed.

(3) The high-pressure valve, the drive valve on the booster pump, the inlet valve of the reaction chamber, and the outlet valve of the gas cylinder were opened. At this point, the gas cylinder, booster pump, and reaction chamber formed a connected system.

(4) The air compressor was then turned on and its outlet valve was opened. The air passed through a filter before entering the booster pump, which drives the booster pump to continuously provide power for the CO_2. The CO_2 from the CO_2 cylinder was gradually injected into the reaction chamber.

(5) By observing the air pressure gauge on the kettle, the inlet valve and pressurization system were closed when the air pressure in the kettle reached the target value. During the actual pressurization and warming process, the temperature and pressure inside the kettle were recorded every 10 min, and the pressure and temperature in the chamber were continuously recorded during the carbonation process as shown in Fig. 3.

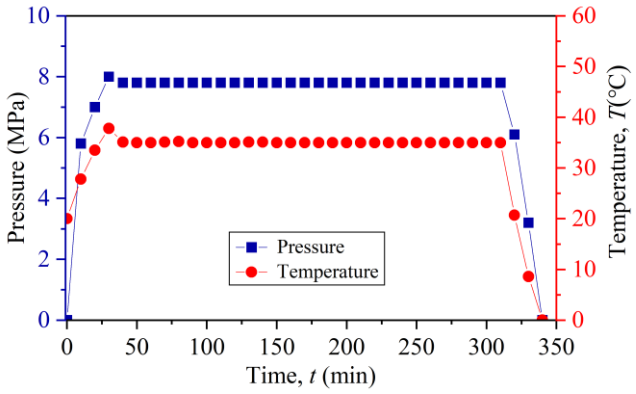

Fig. 3. The curve of temperature and pressure of M-R0.4-S0.50 with time.

2.5. Characterization method for carbonation degree

After the carbonation test was completed, the specimen was cut into two halves from the center. The resulting section was then blown with a washing ball to remove any residual powder. A 1% phenolphthalein solution, prepared according to the carbonation test method outlined in the standard for test method of long term performance and durability of ordinary concrete [49], was sprayed onto the concrete surface. After 30 seconds, the uncarbonated portion turned purple, while the fully carbonated area remained colorless. The carbonation depth of each point is measured by using a vernier caliper with a 10 mm interval as the measurement point. The carbonation depth is calculated according to Eq. (2):

$$d = \frac{1}{n}\sum_{i=1}^{n} d_i \tag{2}$$

where d is the average carbonation depth (mm), d_i is the carbonation depth at each measurement point (mm), n is the total number of measurement points.

2.6. Microscopic test of cementitious materials before and after supercritical carbonation

2.6.1. Scanning electron microscope observations

To investigate the microstructure of cementitious materials before and after supercritical carbonation, both uncarbonated and carbonated samples were ground, and particles approximately 2 mm in size were selected. The selected particles were oven-dried at 60 °C for 24 hours and then sequentially polished from coarse to fine using metallographic sandpaper until a mirror-like surface was achieved. Subsequently, a thin gold (Au) coating was applied to the specimen surface using a JFC-1600 sputter coater to minimize image distortion or brightness artifacts caused by charge accumulation during SEM observation. A JSM-7500F scanning electron microscope (SEM) from JEOL was used to observe the crystal morphology and pore

structure of the samples before and after supercritical carbonation at a 20 kV accelerating voltage, with a magnification set at 20000×. EDX analysis was also performed by using Shimadzu's EDX-7000 X-ray fluorescence analyzer.

2.6.2. DSC-TGA measurement

To investigate the variations in $CaCO_3$ and $Ca(OH)_2$ contents between the carbonated and non-carbonated zones of cement-based materials under supercritical CO_2 conditions, samples from both zones were separately crushed and ground into powder. A STA449F5 simultaneous thermal analyzer from Netzsch (Germany) was used to perform thermogravimetric analysis (TGA) on the samples. Prior to DSC-TGA analysis, the cementitious materials were dried at 40 °C for 12 hours, pulverized, and sieved through an 80 μm square-mesh sieve; the resulting powders were subsequently subjected to thermal analysis. During the test, nitrogen was used as the purge gas to heat the sample to 1000 °C at a rate of 10 °C/min, while changes in sample mass were continuously monitored.

3. Results and discussion

3.1. Pore water saturation distribution of cementitious materials

To achieve uniform control of pore water saturation in mortar and concrete specimens with different water to cement ratios (w/c), the ratio of the mass difference between the saturated state (m_s) and the oven-dried state (m_0) to the oven-dried mass (m_0) was calculated as the average water content of the specimens. Based on these calculations, average water content curves for mortar and concrete specimens with varying w/c ratios were plotted, as shown in Figure 4. The figure illustrates the average water content of mortar and concrete specimens with w/c ratios of 0.4, 0.5, and 0.6 under saturated conditions. The average water content for saturated mortar specimens was 8.1%, 8.8%, and 9.3%, respectively, while for concrete specimens, it was 5.2%, 5.7%, and 6.4%, respectively.

It can be observed that for the same w/c ratio, the water content of mortar specimens was higher than that of concrete specimens. This difference arises because concrete contains coarse aggregates, resulting in a lower proportion of sand compared to mortar. Sand has a larger specific surface area, allowing it to adsorb and retain more water, whereas coarse aggregates, with their smaller specific surface area, exhibit relatively lower water absorption. Additionally, as the w/c ratio decreases, the water content of both concrete and mortar specimens slightly declines. This is due to the increased strength and denser pore structure at lower w/c ratios, which reduces the volume available for water storage within the pores.

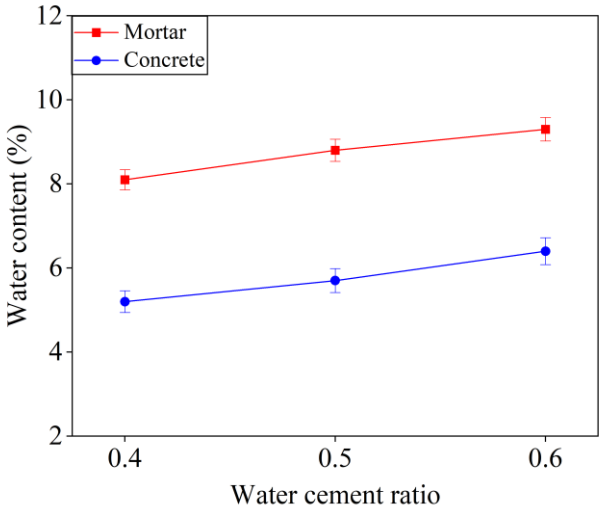

Fig. 4. Water content of mortar and concrete at full saturation for different water-cement ratios.

According to the method described in Section 2.3, water-saturated specimens were oven-dried for varying durations. After each drying interval, three specimens were removed, weighed, and their average value of pore water saturation at each drying time point was calculated using Equation (1). The fitted curves were then plotted, as shown in Figures 5(a-b). Figures 5(a-b) display scatter plots of pore water saturation for mortar and concrete specimens with different water to cement ratios (w/c) at various drying times. By fitting the drying curves for specimens with w/c ratios of 0.4, 0.5, and 0.6, six similar exponential function curves were obtained, indicating that the w/c ratio has minimal effect on the changes in pore water saturation during the drying process of cementitious materials [50].

Additionally, the drying curves of mortar and concrete specimens exhibit similar trends, suggesting that the internal aggregates have a negligible influence on pore water saturation during drying. Throughout the drying process, pore water saturation initially decreases rapidly and then gradually levels off. This behavior occurs because, as a porous material, the surface pore water of concrete evaporates more readily, while the internal pore water must first diffuse to the surface. As drying time increases, this diffusion process slows down, leading to a gradual reduction in the rate of change in pore water saturation.

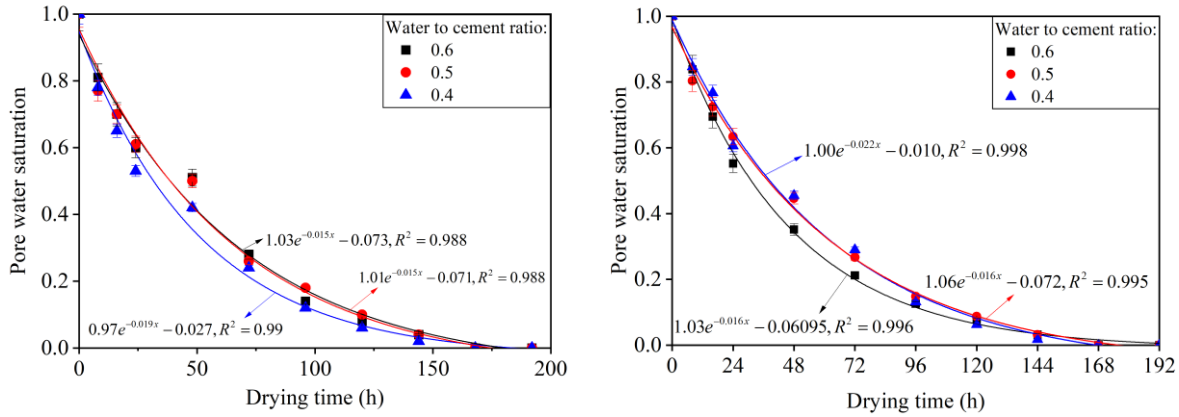

(a) Cement mortar (b) Concrete

Fig. 5. Drying curves of specimens with different water-cement ratios after saturation at 60°C.

Based on the predictive formula presented in Figures 5(a-b), the drying time required for specimens to reach the target pore water saturation was calculated. The results, as shown in Table 4, detail the drying times needed for mortar and concrete specimens with water to cement ratios of 0.4, 0.5, and 0.6 to achieve target pore water saturation levels of 0.40, 0.50, 0.60, and 0.70.

Table 4

Drying time used to dry the specimen to the target pore water saturation (h).

Specimen number	Target pore water saturation			
	0.40	0.50	0.60	0.70
M-R0.4	42.38	31.56	22.63	15.03
M-R0.5	51.68	38.64	27.71	18.30
M-R0.6	51.27	38.61	27.99	18.84
C-R0.4	41.19	31.12	22.86	15.85
C-R0.5	50.42	38.45	28.42	19.78
C-R0.6	49.93	37.71	27.51	18.74

At this stage, the pore water saturation at different depths within the cementitious material specimens was still uneven. To achieve a uniform distribution of pore water saturation, the dried specimens were placed in a constant temperature and humidity curing chamber with the target humidity, following the method described in Section 2.3. The temperature was set at 20°C, and the specimens underwent wet steady-state pretreatment for 30 days to ensure uniform pore water distribution and achieve the target saturation level [22,46,47]. These specimens, with uniformly distributed pore water saturation, were then subjected to supercritical carbonation tests.

3.2. Carbonation depth of cementitious materials under supercritical CO_2 condition

3.2.1. Effect of pore water saturation

After processing the cement mortar and concrete specimens to achieve a uniform distribution of the different target pore water saturations, supercritical carbonation tests were conducted following the method described in Section 2.4. Variations in internal pore water saturation inevitably affect the diffusion rate of CO_2 during carbonation, thereby influencing the progress of the supercritical carbonation reaction and ultimately the carbonation results. To investigate the impact of different pore water saturation on the supercritical carbonation of cement mortar and concrete specimens, part of the specimens were tested for carbonation depth using the method in Section 2.5. The results are shown in Figure 6, and the carbonation depths calculated using Equation (2) are presented in Figure 7.

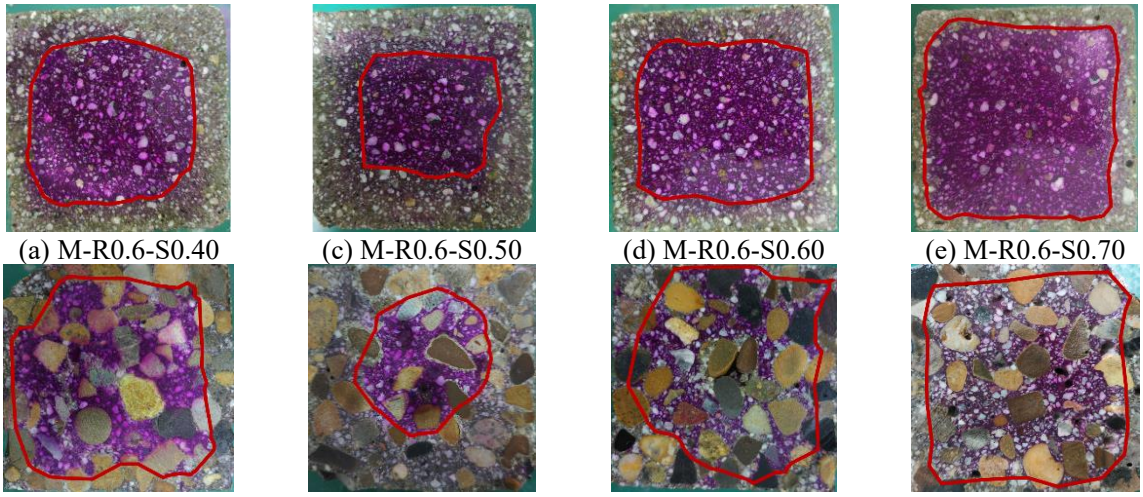

(a) M-R0.6-S0.40 (c) M-R0.6-S0.50 (d) M-R0.6-S0.60 (e) M-R0.6-S0.70

(f) C-R0.6-S0.40 (h) C-R0.6-S0.50 (i) C-R0.6-S0.60 (j) C-R0.6-S0.70

Fig. 6. Supercritical carbonation boundaries for cement mortar and concrete with different pore water saturations.

Fig. 7 shows the carbonation depth of cement mortar and concrete specimens under different pore water saturation conditions after processing with uniform pore water distributions, followed by the application of a phenolphthalein ethanol indicator. The relationship between supercritical carbonation depth and pore water saturation obtained from the tests for both cement mortar and concrete was nonlinearly fitted, as shown in Figure 7. The fitting results indicate that the carbonation depth reaches its maximum at a pore water saturation of 0.50. In addition, some experimental results of concrete and cement mortar were statistically summarized and drawn together in Fig. 7. References [22] and [23] present the carbonation results for cement mortar with a water-cement ratio of 0.63 and concrete with a water-cement ratio of 0.4, respectively. From Fig. 7, the following conclusions can be drawn:

(1) No significant supercritical carbonation under fully dry or fully saturated conditions. 1) Fully dry condition: In the fully dry state, there is almost no water in the pores, and carbonation reactions require water as a medium. CO_2 must dissolve in water to form H_2CO_3, which then reacts with $Ca(OH)_2$ in the cement

303 matrix to form $CaCO_3$. The lack of water prevents the reaction from occurring, and carbonation does not take
304 place. 2) Fully saturated condition: In a fully saturated state, the pores are completely filled with water, which
305 obstructs the diffusion of CO_2 gas through the pores. CO_2 cannot diffuse into the specimen through the liquid
306 water to react with $Ca(OH)_2$, so the carbonation reaction either does not occur or happens very slowly.
307 Additionally, at high saturation levels, water acts as a protective barrier to the material in the pores, further
308 reducing the possibility of the reaction.

309 (2) Carbonation depth under supercritical conditions follows a trend of first increasing and then
310 decreasing with increasing pore water saturation. The trend of carbonation depth observed in this study under
311 supercritical conditions is consistent with that reported in the literature for accelerated carbonation, with both
312 reaching maximum carbonation depth at a pore water saturation of 0.5. However, the influence of pore water
313 saturation on carbonation depth is more obvious under supercritical carbonation compared to accelerated
314 carbonation. When the pore water saturation is 0.50, the maximum carbonation depth for mortar and concrete
315 specimens under supercritical carbonation conditions is reached, with values of 16.35 mm and 17.23 mm,
316 respectively. As the pore water saturation increases to 0.70, the carbonation depth of concrete approaches
317 zero. This trend is mainly due to the dual role of pore water in the carbonation process: 1) At low pore water
318 saturation levels, a small amount of water in the pores facilitates the dissolution of CO_2, forming carbonic
319 acid that reacts with $Ca(OH)_2$ to form $CaCO_3$. This promotes increased carbonation depth. 2) At higher pore
320 water saturation levels, the pores are progressively filled with more water, significantly hindering the
321 diffusion of CO_2 gas through the pore network. As CO_2 diffusion is key to sustaining carbonation reactions,
322 the restricted diffusion at higher saturation levels reduces the carbonation rate and depth.

323 Although this study achieved a uniform distribution of pore water saturation within cement mortar and
324 concrete, the generalizability of methods for achieving uniform pore water saturation in cementitious
325 materials remains limited. The multiscale pore structure of cementitious materials, encompassing gel pores,
326 capillary pores, and inter-aggregate voids, results in non-uniform pore water saturation due to varying water
327 retention capacities.

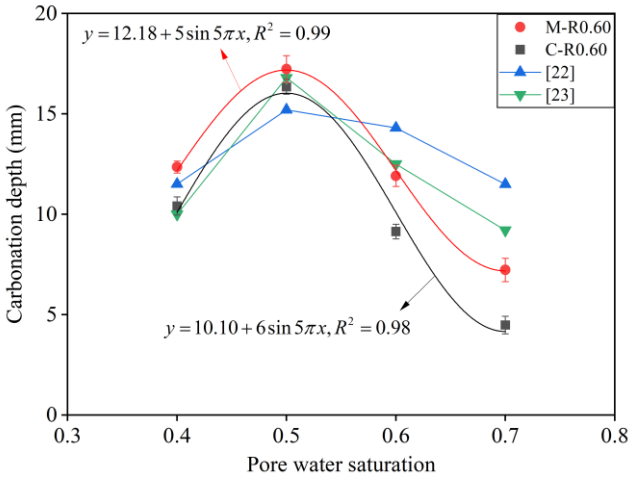

Fig. 7. Supercritical carbonation depth of specimens at different pore water saturation.

3.2.2. *Effect of water to cement ratio*

To maintain generality, Figure 8 shows the supercritical carbonation depth of cement mortar and concrete specimens with different water-cement ratios, processed at a pore water saturation of 0.50. The experimentally derived linear fits of supercritical carbonation depth versus water-cement ratio for cement mortar and concrete are presented in Figure 9. Additionally, data from relevant literature have been incorporated into Figure 9 for comparison. References [26], [27], and [28] present the carbonation results for concrete with pore water saturation levels of 0.8, 0.65, and 0.7, respectively. Reference [29] reports the carbonation results for cement mortar at a pore water saturation of 0.43.

As shown in Figure 9, the carbonation depth observed in this study is significantly greater than that reported for conventional accelerated carbonation in the literature. This difference can be attributed to the much faster reaction kinetics and sharply increased CO_2 diffusion rate under supercritical conditions, which collectively enhance the carbonation depth. Nevertheless, the overall trend of carbonation depth variation remains similar. It can be observed that as the water-cement ratio increases, the supercritical carbonation depth of both cement mortar and concrete increases, and the carbonation depth has a nearly linear relationship with the water-cement ratio. This may be due to the following reasons: (1) Higher water-cement ratio leads to higher porosity: As the water-cement ratio increases, the moisture content in the cement-based materials also increases, which typically results in a more porous structure in the cement paste. A higher water-cement ratio increases the porosity, providing more channels for CO_2 to diffuse. This helps accelerate the carbonation reaction and leads to deeper carbonation. (2) Lower compactness of cement-based materials: A higher water-cement ratio generally leads to a decrease in the compactness of cement-based materials. Lower strength and compactness mean larger pores and looser pore walls, allowing CO_2 to more easily enter and react with

$Ca(OH)_2$ in the cement matrix, further enhancing the carbonation reaction. (3) More reaction medium (water): A higher water-cement ratio results in more water in the pores, which not only provides a medium for CO_2 dissolution but also increases the opportunity for CO_2 to react with $Ca(OH)_2$ in the cement matrix, thereby accelerating the carbonation process.

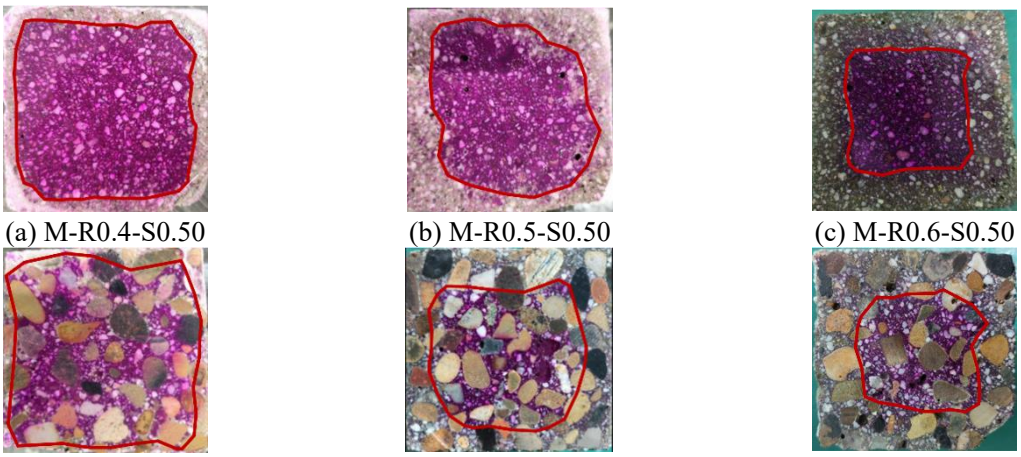

(a) M-R0.4-S0.50 (b) M-R0.5-S0.50 (c) M-R0.6-S0.50

(d) C-R0.4-S0.50 (e) C-R0.5-S0.50 (f) C-R0.6-S0.50

Fig. 8. Supercritical carbonation boundaries for cement mortars and concrete with different water-cement ratios.

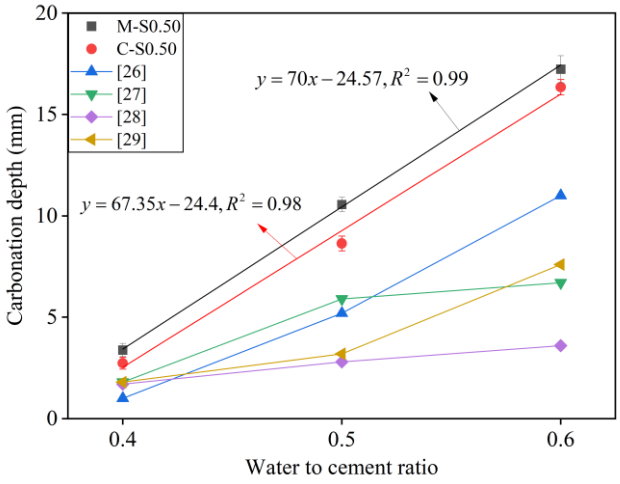

Fig. 9. Supercritical carbonation depth of specimens with different water-cement ratios.

3.3. Microstructural evolution of cementitious materials under supercritical CO_2 condition

3.3.1. Microstructure of cementitious materials

To study the microstructural changes in cementitious materials before and after supercritical carbonation, samples of both uncarbonated and carbonated materials were crushed and ground into powder following the carbonation test. The crystal morphology and pore structure of the samples before and after supercritical

carbonation were observed using a scanning electron microscope according to the method in Section 2.6.1, with a magnification of 20,000 times. The elemental composition was also analyzed.

Without loss of generality, SEM images and EDX analyses of cement mortar specimens with a water-cement ratio of 0.6 and a pore water saturation of 0.50, both uncarbonated and carbonated, are shown in Figures 10 and 11, respectively.

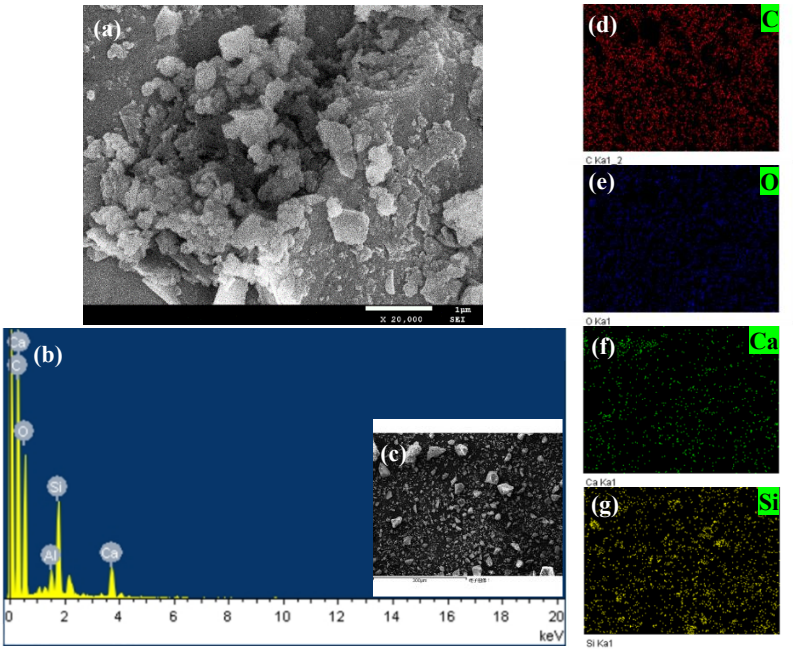

Fig. 10. Chemical composition of uncarbonated cement mortar (M-R0.6-S0.50). (a) SEM images, (b) Elements distribution, (d)-(g) Elemental surface sweeps across the region in Fig. (c).

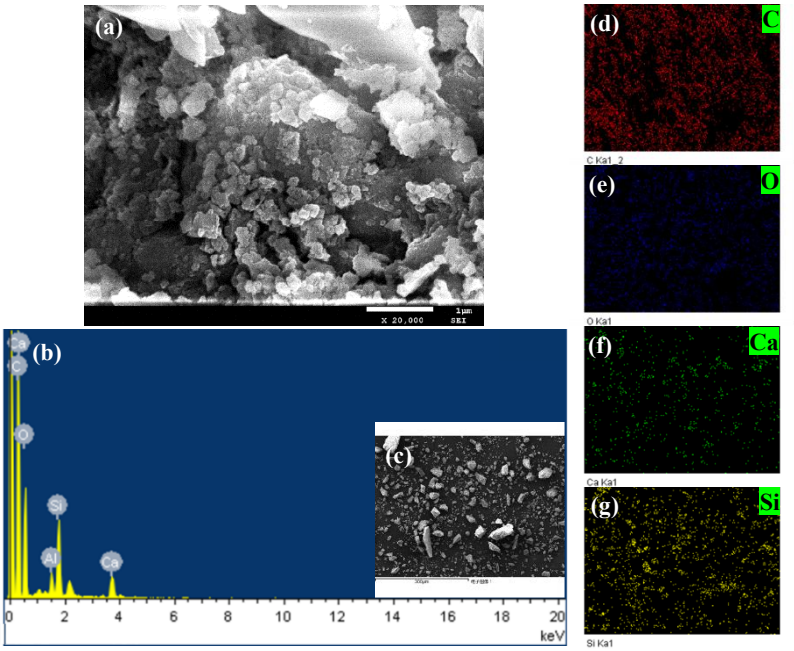

Fig. 11. Chemical composition of carbonated cement mortar (M-R0.6-S0.50). (a) SEM images, (b) Elements distribution, (d)-(g) Elemental surface sweeps across the region in Fig. (c).

In addition, SEM images and EDX elemental compositions of fully carbonated and uncarbonated concrete specimens were also tested and the results were plotted as shown in Figure 12. SEM images reveal internal hydration products (Aft, C-S-H, $Ca(OH)_2$) before carbonation and carbonation products ($CaCO_3$) with lamellar or flaky morphology after carbonation, making the structure denser. However, $CaCO_3$ accumulation is not uniform and shows some randomness. Elemental analysis via EDX showed that in the fully carbonated area, the C element content increased significantly compared to the uncarbonated sample, while the Ca element content decreased, leading to a higher C/Ca atomic ratio. This indicates a higher degree of carbonation, implying that besides the carbonation of $Ca(OH)_2$, the carbonation of C-S-H also occurred.

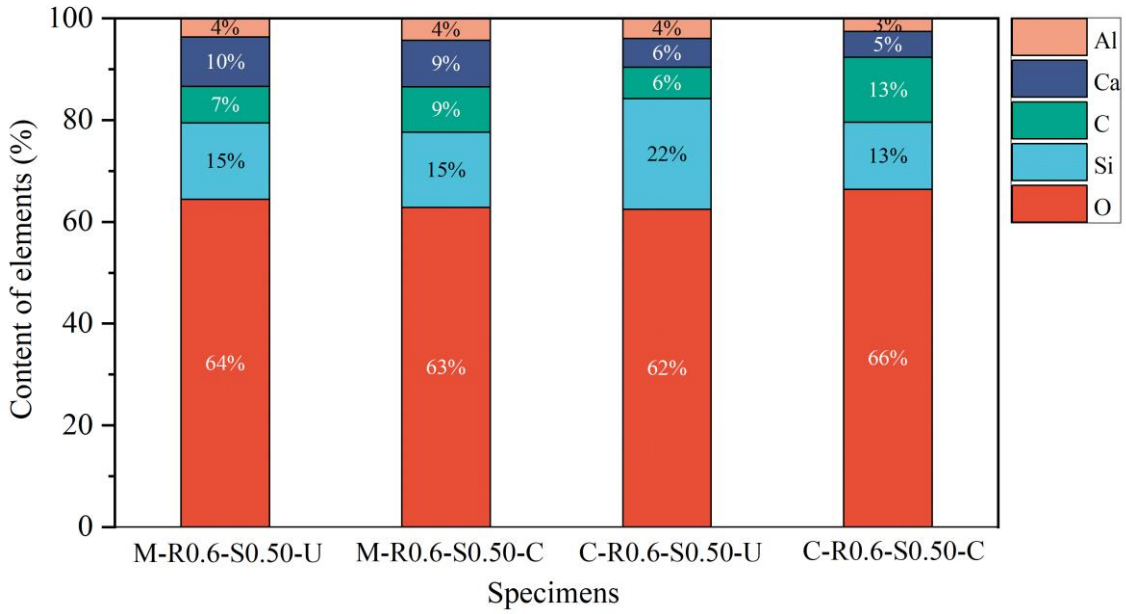

Fig. 12. EDX analysis of element composition.

Remarks: U and C denotes the uncarbonated and carbonated sample, respectively.

3.3.2. Contents of $Ca(OH)_2$ and C-S-H

To examine the variations in $Ca(OH)_2$ and C-S-H contents within the carbonation and non-carbonation zones of cementitious materials under supercritical CO_2 conditions, samples from both zones were separately crushed, ground into powder, and analyzed using the DSC-TGA test, following the procedure outlined in Section 2.6.2. For each experimental condition investigated in this study, three replicate specimens were prepared and analyzed using TGA. Without loss of generity, only one representative TGA result per condition is presented and shown in Fig. 13. As shown in Fig. 13, an obviously increase in the weight loss gradient is observed between 550 °C and 900 °C following carbonation, primarily due to the elevated $CaCO_3$ content in the cementitious matrix. Notably, a mass loss in the same temperature range is also evident in the uncarbonated sample, suggesting that $CaCO_3$ was already present in the aggregates prior to carbonation [51].

To address the interference caused by the inherent $CaCO_3$ in the aggregates, it is assumed that the components within the sample are uniformly distributed prior to carbonation. Based on this assumption, phase subtraction between TGA curves before and after carbonation can be performed to accurately quantify the amount of $CaCO_3$ generated by the supercritical carbonation reaction. This approach enables a more precise assessment of the carbon sequestration capacity of cementitious materials treated under supercritical conditions.

To ensure the accuracy of the test results and mitigate potential interference from $CaCO_3$ present in the aggregates of the cementitious material, the TGA results of the specimens before and after carbonation were subtracted, and the difference was plotted as curves, as illustrated in Fig. 14. Generally, the temperature range of 400℃-550℃ can be attributed to mass loss resulting from $Ca(OH)_2$ decomposition [52], while the range of 550℃-900℃ corresponds to mass loss due to $CaCO_3$ decomposition [53]. Additionally, the decomposition peak of C-S-H occurs at approximately 100℃ [53].

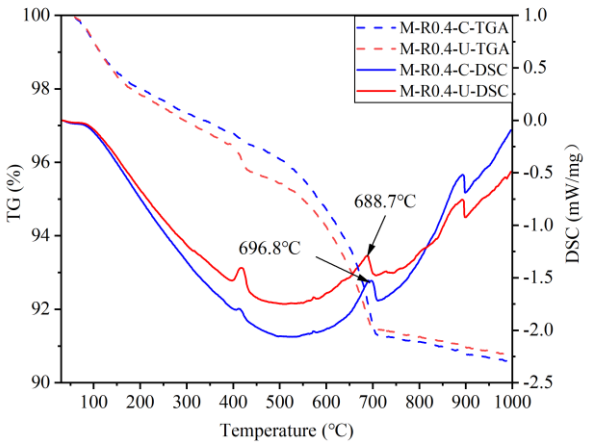

(a) M-R0.4

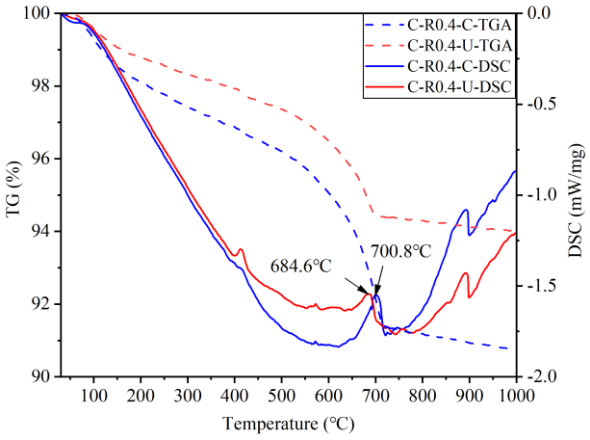

(b) C-R0.4

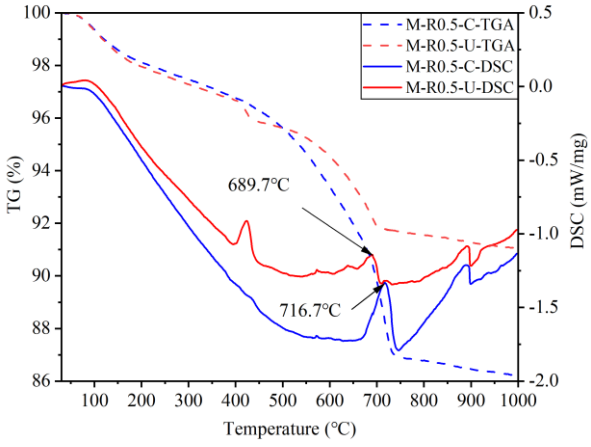

(c) M-R0.5

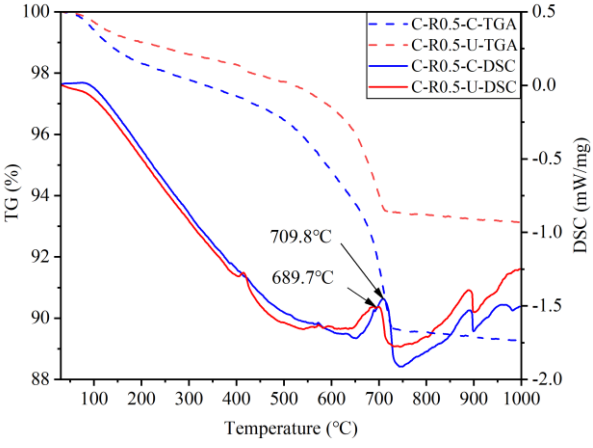

(d) C-R0.5

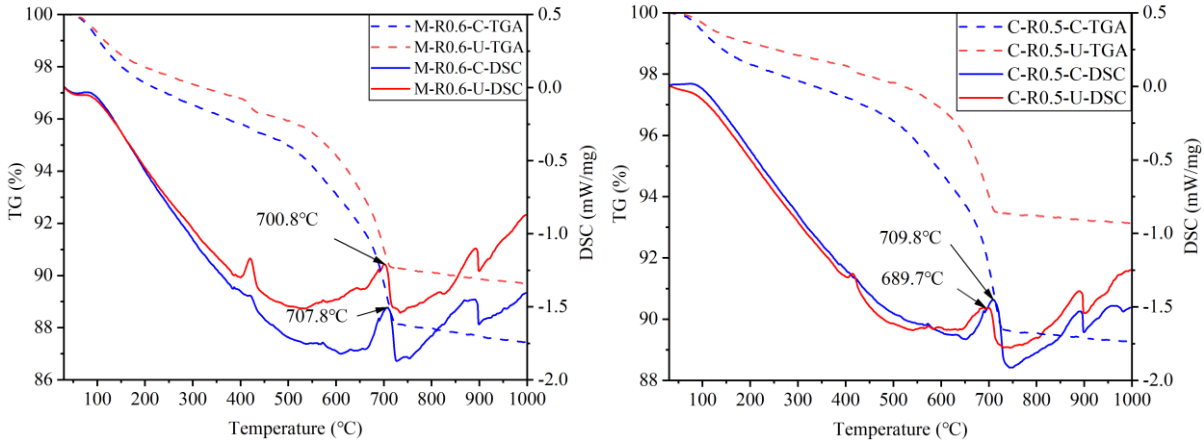

(e) M-R0.6 (f) C-R0.6

Fig. 13. TGA test results of cement mortar and concrete

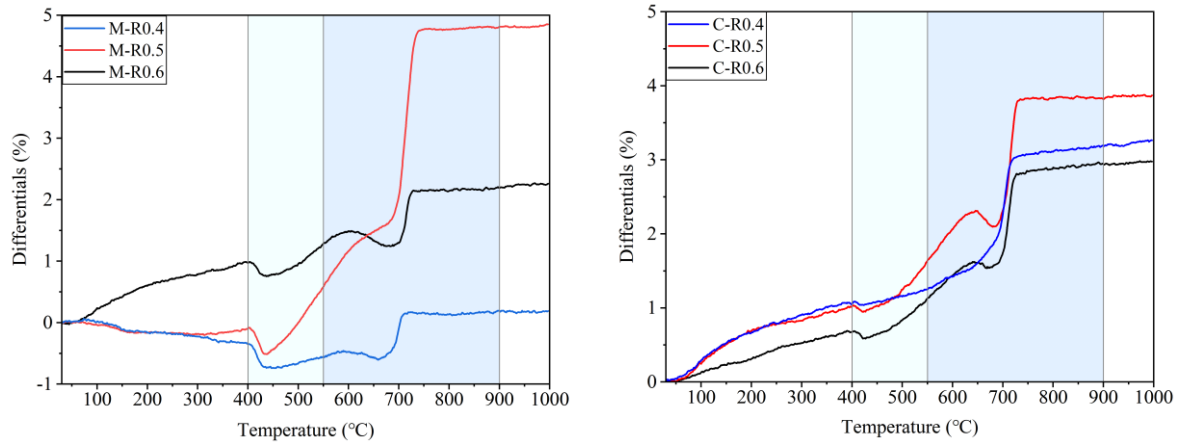

(a) Cement mortar (b) Concrete

Fig. 14. Differences(the result of subtraction) in TGA results of cement mortar and concrete before and after supercritical carbonation.

Previous research has indicated that in the carbonation model of mature concrete, the carbonation of unhydrated minerals can be neglected, with $Ca(OH)_2$ and C-S-H being the primary reactants in the carbonation process [4]. Consequently, it is assumed that all $CaCO_3$ formed during the supercritical carbonation reaction originates from $Ca(OH)_2$ and C-S-H. Furthermore, it has been reported that the Ca/Si ratio in the molecular structure of C-S-H is 1.5, and its chemical formula is represented as $3CaO{\cdot}2SiO_2{\cdot}3H_2O$ [5]. The phenolphthalein indicator, which decolorizes below pH 8.2, was used to assess carbonation. This decoloration corresponds to the depletion of $Ca(OH)_2$ and the resulting pH drop to near-neutral levels. EDX analysis further confirmed carbonation, showing a Ca/C atomic ratio close to 1:1, indicating the formation of $CaCO_3$ and full carbonation of the carbonated zone. These complementary results confirm that the specimens had reached full carbonation under the test conditions.

To identify the contents of $CaCO_3$ and $Ca(OH)_2$, this study proposes a novel calculation method based

on the supercritical carbonation approach to determine the C-S-H and $Ca(OH)_2$ contents in cementitious materials before carbonation. The $CaCO_3$ formed through complete carbonation primarily originates from the hydration products $Ca(OH)_2$ and C-S-H. By utilizing TGA test results to quantify the $CaCO_3$ produced by the carbonation reaction and the amount of $Ca(OH)_2$ involved, the portion of $CaCO_3$ derived from $Ca(OH)_2$ can be determined. The remaining fraction of $CaCO_3$ is attributed to C-S-H, allowing for the inverse deduction of the initial C-S-H and $Ca(OH)_2$ contents before carbonation.

The mass of $CaCO_3$ produced by the carbonation reaction was determined by multiplying the mass of the specimen used in the TGA test by the mass loss observed between 550°C and 900°C in the curve of Fig. 13, as described in Eq. (3). Similarly, the mass of $Ca(OH)_2$ involved in the carbonation reaction was calculated by multiplying the mass of the specimen by the mass loss between 400°C and 550°C in the curve of Fig. 13, as shown in Eq. (4). The mass of $CaCO_3$ derived from $Ca(OH)_2$ was obtained by multiplying the ratio of the mass of $Ca(OH)_2$ to its molar mass by the molar mass of $CaCO_3$, as expressed in Eq. (5). The remaining portion of $CaCO_3$ is derived from C-S-H, and its mass, relative to the molar mass of $CaCO_3$, is multiplied by the molar mass of C-S-H. Given that C-S-H is assumed to have the chemical composition of $3CaO{\cdot}2SiO_2{\cdot}3H_2O$ [5], the resulting value is then divided by 3 to determine the mass of C-S-H involved in the carbonation reaction, as presented in Eq. (6). Subsequently, the mass fraction of $Ca(OH)_2$ is calculated as the ratio of the mass of $Ca(OH)_2$ to the total mass of $Ca(OH)_2$ and C-S-H, as shown in Eq. (7). Finally, the mass fraction of C-S-H is obtained by subtracting the mass fraction of $Ca(OH)_2$ from 1, as given in Eq. (8).

$$m_{CC} = \left(D_{900} - D_{550}\right) \times m \tag{3}$$

$$m_{CH} = \left(D_{550} - D_{400}\right) \times m \tag{4}$$

$$m_{CH \to CC} = \frac{m_{CH}}{M_{CH}} \times M_{CC} \tag{5}$$

$$m_{C-S-H} = \frac{m_{CC} - m_{CH \to CC}}{3M_{CC}} M_{C-S-H} \tag{6}$$

$$P_{CH} = \frac{m_{CH}}{m_{CH} + m_{C-S-H}} \tag{7}$$

$$P_{C-S-H} = 1 - P_{CH} \tag{8}$$

where D_{900}, D_{550}, D_{400} represent the mass loss at 900°C, 550°C and 400°C, respectively, as determined by the TGA test. m is the mass of the powder sample used in the TGA test. m_{CC} refers to the total mass of $CaCO_3$

produced by the carbonation reaction, while m_{CH} denotes the mass of $Ca(OH)_2$ involved in the carbonation reaction. $m_{CH\rightarrow CC}$ represents the mass of $CaCO_3$ derived from $Ca(OH)_2$. The molar mass of $Ca(OH)_2$ (M_{CH}) is 74 g/mol, whereas the molar mass of $CaCO_3$ (M_{CC}) is 100 g/mol. Additionally, $m_{C\text{-}S\text{-}H}$ signifies the mass of C-S-H involved in the carbonation reaction, with its molar mass ($M_{C\text{-}S\text{-}H}$) being 342 g/mol. The percentage content of $Ca(OH)_2$ and C-S-H are denoted as P_{CH} and $P_{C\text{-}S\text{-}H}$, respectively.

The contents of $Ca(OH)_2$ and C-S-H in cementitious materials prior to carbonation were determined using this calculation method, and the average value was calculated with the error range plotted as shown in Fig. 15. Currently, the exact ratio of $Ca(OH)_2$ and C-S-H in cementitious materials is not directly available in the literature. Most researchers estimate that C-S-H accounts for approximately 70% of the cementitious matrix [54-56], while some studies suggest that the $Ca(OH)_2$ content is only around 20% [57], which aligns well with the calculated results based on Eqs (3)-(7). Accurate determination of the $Ca(OH)_2$ and C-S-H contents in cementitious materials is essential for evaluating their carbon sink capacity. It also enables more precise prediction of the supercritical carbonation rate and depth, while contributing to the improvement of numerical models for the supercritical carbonation of cementitious materials.

Although the contents of $Ca(OH)_2$ and C-S-H in cementitious materials can be calculated, secondary hydration reactions of the raw materials may affect the accurate assessment of $Ca(OH)_2$ and C-S-H content before and after supercritical carbonation. These reactions typically result in a decrease in $Ca(OH)_2$ and an increase in C-S-H formation.

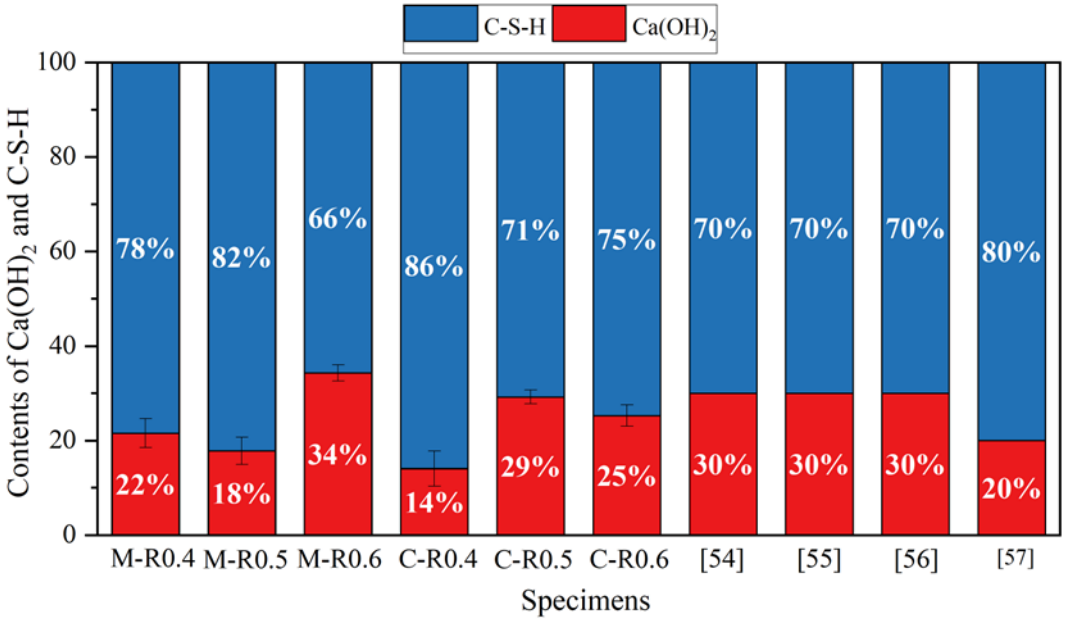

Fig. 15. $Ca(OH)_2$ and C-S-H contents in cementitious materials before supercritical carbonation.

3.4. Carbon-sink capacity of cementitious materials after supercritical carbonation treatment

By eliminating the influence of $CaCO_3$ present in the internal aggregate, the amount of $CaCO_3$ formed through carbonation can be accurately quantified, allowing for a precise assessment of the CO_2 storage capacity in fully carbonated cementitious materials. The first step involves calculating the mass of $CaCO_3$ produced per cubic meter of concrete, which is obtained by multiplying the mass loss between 550°C and 900°C in the curve of Figure 14 by the mass of one cubic meter of concrete. This result is then divided by the molar mass of $CaCO_3$ and subsequently multiplied by the molar mass of CO_2 to determine the mass of CO_2 absorbed per cubic meter of carbonated concrete, as expressed in Eq. (8). The CO_2 uptake of the cementitious material was then calculated using Eq. (8), and the results are presented in Figure 16.

$$m_{CO_2} = \frac{(D_{900} - D_{550})m_C}{M_{CC}} M_{CO_2} \tag{8}$$

where m_{CO2} represents the mass of CO_2 absorbed per cubic meter of concrete, m_C denotes the mass of concrete per cubic meter (2400 kg/m^3), and M_{CO2} is the molar mass of CO_2 (44 g/mol).

As shown in Figure 16, Reference [58] corresponds to concrete produced by CarbonCure (Canada); Reference [59] describes a novel carbonated CO_2-fly ash-based backfill (CFBF); Reference [60] details a carbonation approach involving CO_2 injection into a cement suspension, which is subsequently used for concrete production; Reference [61] pertains to CO_2-foamed concrete (CFC); and Reference [62] discusses carbon sequestration in recycled coarse aggregates. The supercritical carbonation treatment of cementitious materials achieves complete carbonation, making it a more promising approach for carbon storage in concrete compared to other methods. The carbon storage capacity of fully carbonated concrete under supercritical conditions is approximately 2-3 times higher than that of other reported values. However, variations in the carbonation degree among different types of concrete inevitably affect their carbon storage capacity. Therefore, further research is needed to develop a relationship model between the carbonation degree of cementitious materials and their carbon storage capacity to enable a more accurate assessment of carbon storage potential of concrete.

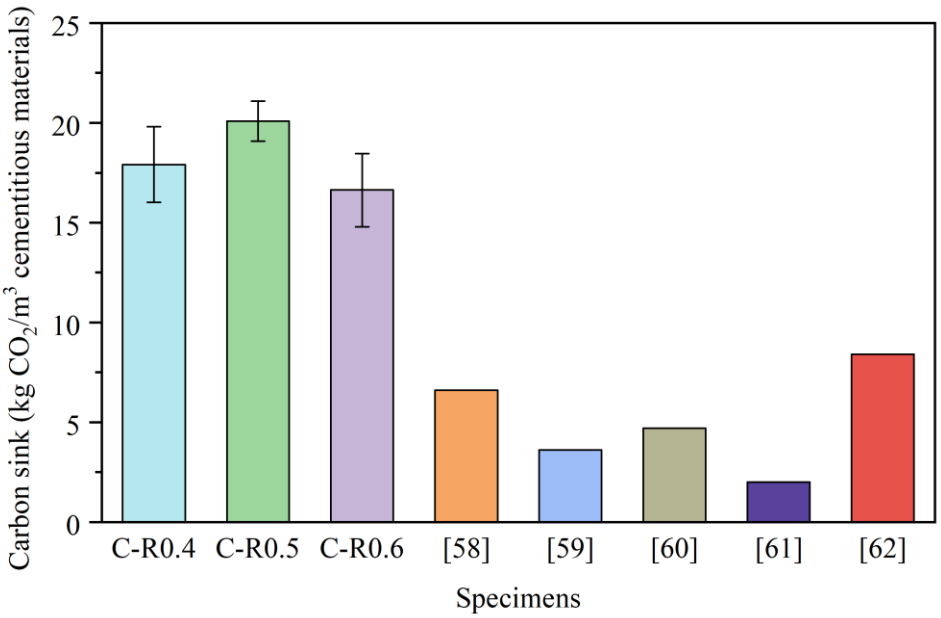

Fig. 16. CO_2 uptake of cementitious materials after completely carbonation.

3.5. Mechanism of supercritical carbonation of cementitious materials

The supercritical carbonation reaction of cementitious materials is a complex process involving multi-physicochemical coupling [7,17,63]. This includes chemical reaction rates during supercritical carbonation, mass conservation in gas-liquid two-phase flow, diffusion and solubility of CO_2 in pore water, and energy conservation in porous media. Fig. 17(a) illustrates the composition of the various phases of the cementitious material, where mass transfer occurs due to temperature and pressure gradients. Fig. 17(b) depicts the dissolution of CO_2 in water, its diffusion, and the chemical reactions that lead to internal carbonation. Cementitious materials can be viewed as porous media consisting of solid, liquid, and gas phases, and under supercritical conditions, CO_2 mass transfer occurs as the pressure gradient drives the liquid flow. The temperature gradient within the material during supercritical carbonation induces heat transfer within the porous medium. Due to the high CO_2 concentration in the pores, only a portion of the gas dissolves in the water, with the dissolved CO_2 undergoing a propagation-diffusion process driven by concentration gradients and liquid flow. Based on the above analysis, supercritical carbonation of cementitious materials can be summarized into the following four main processes: carbonation reaction, propagation and diffusion of CO_2 dissolved in water, mass transfer of liquid and gas, and energy balance in porous media.

Figure 17(c) illustrates the mechanism by which pore water saturation affects the supercritical carbonation process of cementitious materials.

(1) When the pore water saturation is low, a portion of the $Ca(OH)_2$ cannot fully undergo the carbonation

reaction because the insufficient moisture prevents complete contact between CO_2 and the reactants. Additionally, the small humidity gradient within the cementitious material weakens the driving force for water evaporation and migration, which hinders the expansion of the carbonation reaction zone. This effect is particularly pronounced in thicker cementitious materials, where low saturation restricts the carbonation reaction to the surface layer, making deep carbonation difficult and resulting in a reduced final carbonation depth.

(2) When the pore water saturation is excessively high, a large number of pores become filled with water, obstructing CO_2 transport. Furthermore, excessive moisture dilutes the concentration of products formed by the carbonation reaction within the cementitious material, thereby reducing the driving force for the reaction and slowing the carbonation rate. High water content may also occupy the reaction sites, inhibiting the carbonation process. Additionally, when pore water saturation is too high, the water gradient within the material diminishes, reducing water migration and hindering CO_2 contact with uncarbonated regions. This can lead to unsustainable carbonation reactions in localized areas, resulting in a decrease in the density and stability of the carbonation layer, which in turn affects the overall carbonation depth of the material.

(3) When the pore water saturation is moderate, it does not block the pore space, allowing for the effective diffusion of CO_2, while also providing sufficient water support for the carbonation reaction. There is neither dilution of the carbonation products due to excess water nor inhibition of the reaction caused by insufficient water. At this point, an appropriate humidity gradient remains within the cementitious material, supporting water evaporation and migration, which helps extend the carbonation reaction to the deeper layers of the concrete. The rate of carbonation product formation is moderate, and the stability of $CaCO_3$ and other products is high, maximizing both the carbonation depth and reaction efficiency. Therefore, achieving the optimal pore water saturation is crucial for the supercritical carbonation reaction.

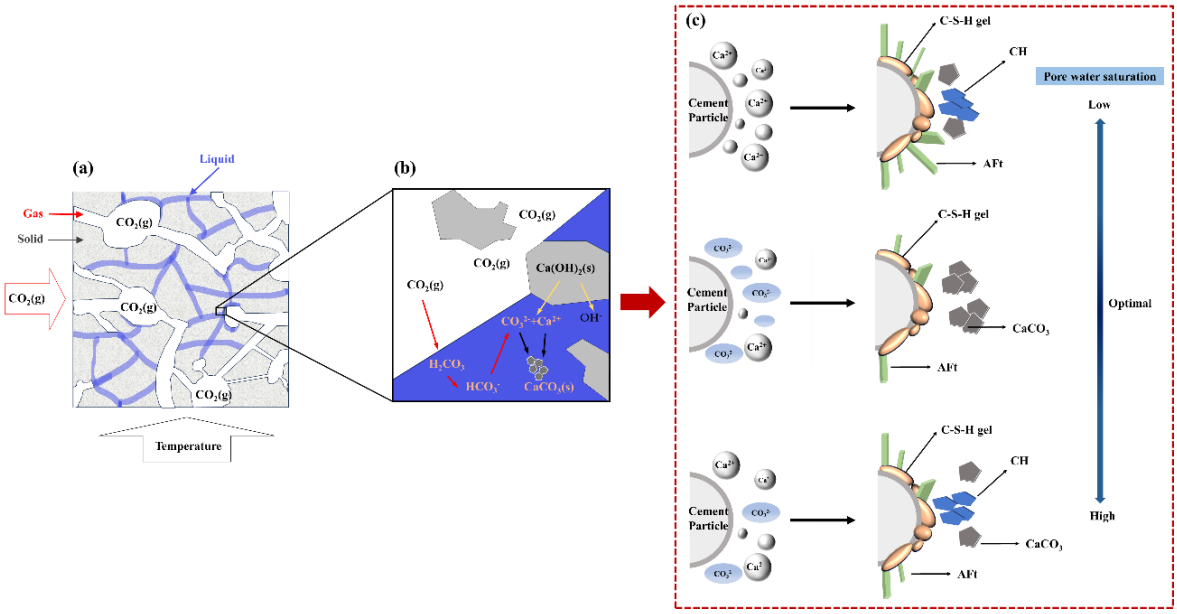

Fig. 17. Mechanism of the effect of pore water saturation on the supercritical carbonation process of cementitious materials.

4. Conclusion

In this study, supercritical carbonation tests were conducted on cement mortar and concrete with varying pore water saturation levels. Carbonation depth measurements were performed to analyze the effects of pore water saturation on the supercritical carbonation process of cement-based materials. Additionally, specimens with different water-cement ratios were subjected to TGA and SEM before and after supercritical carbonation to investigate the reaction mechanism and develop a calculation method for $Ca(OH)_2$ and C-S-H contents. Based on the findings, the following conclusions can be drawn:

(1) A method was proposed for accurately regulating the pore water saturation of cementitious materials to a specific target value with a uniform distribution.

(2) As pore water saturation increases, the supercritical carbonation depth of cementitious materials first increases and then decreases, reaching its maximum at a pore water saturation of 0.50. When the water-cement ratio ranges between 0.4 and 0.6, the supercritical carbonation depth increases linearly with the water-cement ratio.

(3) Based on the differences in TGA test results before and after the supercritical carbonation reaction, a method was proposed for the reverse derivation calculation of $Ca(OH)_2$ and C-S-H content in cementitious materials prior to carbonation.

(4) Pore water saturation influences the supercritical carbonation process of cementitious materials by affecting CO_2 transport, reaction kinetics, and carbonation depth, with optimal carbonation efficiency

occurring at moderate saturation levels.

(5) Future research will focus on replacing natural aggregates with recycled ones and substituting cement with SCMs to utilize solid waste, reduce cement usage, enhance CO_2 sequestration, improve concrete performance, and lower costs.

References

[1] Liu Z, Meng W (2021) Fundamental understanding of carbonation curing and durability of carbonation-cured cement-based composites: A review. Journal of CO_2 Utilization 44: 101428. https://doi.org/10.1016/j.jcou.2020.101428

[2] Liu ZX, Sun CC, Qu J (2024) Coupling Effects of Stress and Carbonation on Concrete Durability: A Review. Mater. 17: 5438. https://doi.org/10.3390/ma17225438

[3] Li L, Mu M (2022) An overview of utilizing CO_2 for accelerated carbonation treatment in the concrete industry. Journal of CO_2 Utilization 60: 102000. https://doi.org/10.1016/j.jcou.2022.102000

[4] Peter MA, Muntean A, Meier SA, Boehm M (2008) Competition of several carbonation reactions in concrete: A parametric study. Cement Concrete Res 38: 1385-1393. https://doi.org/10.1016/j.cemconres.2008.09.003

[5] Liu X, Feng P, Cai Y, Yu X, Yu C, Ran Q (2022) Carbonation behavior of calcium silicate hydrate (C-S-H): Its potential for CO_2 capture. Chemical Engineering Journal 431: 134243. https://doi.org/10.1016/j.cej.2021.134243

[6] Morandeau A, Thiery M, Dangla P (2014) Investigation of the carbonation mechanism of CH and CSH in terms of kinetics, microstructure changes and moisture properties. Cement Concrete Res 56: 153-170. https://doi.org/10.1016/j.cemconres.2013.11.015

[7] Phung QT, Maes N, Jacques D, Schutter GD, Ye G, Perko J (2016) Modelling the carbonation of cement pastes under a CO_2 pressure gradient considering both diffusive and convective transport. Constr Build Mater 114: 333-351. https://doi.org/10.1016/j.conbuildmat.2016.03.191

[8] Stefanoni M, Angst U, Elsener B (2018) Corrosion rate of carbon steel in carbonated concrete – A critical review. Cement Concrete Res 103: 35-48. https://doi.org/10.1016/j.cemconres.2017.10.007

[9] Fuhaid A, Fahad A, Niaz A (2022) Carbonation and corrosion problems in reinforced concrete structure. Build 12(5): 586. https://doi.org/10.3390/buildings12050586

[10] Mo L, Panesar DK (2013) Accelerated carbonation-A potential approach to sequester CO_2 in cement paste containing slag and reactive MgO. Cement Concr. Compos. 43: 69-77. https://doi.org/10.1016/j.cemconcomp.2013.07.001

[11] Yuan Q, Zhang Y, Wang T, Wang J (2023) Characterization of heavy metals in fly ash stabilized by carbonation with supercritical CO_2 coupling mechanical force. Journal of CO_2 Utilization 67: 102308. https://doi.org/10.1016/j.jcou.2022.102308

[12] Zhan B, Poon C, Shi C (2013) CO_2 curing for improving the properties of concrete blocks containing recycled aggregates. Cement Concr. Compos. 42: 1-8. https://doi.org/10.1016/j.cemconcomp.2013.04.013

[13] Kou SC, Zhan B, Poon CS (2014) Use of a CO_2 curing step to improve the properties of concrete prepared with recycled aggregates. Cement Concr. Compos. 45: 22-28. https://doi.org/10.1016/j.cemconcomp.2013.09.008

[14] Santos SF, Schmidt R, Almeida A, Tonoli G, Savastano H (2015) Supercritical carbonation treatment

on extruded fibre – cement reinforced with vegetable fibres. Cement Concr. Compos. 56: 84-94. https://doi.org/10.1016/j.cemconcomp.2014.11.007
[15] Zhang J, Shi C, Li Y, Ran X, Poon CS, Xie Z (2015) Influence of carbonated recycled concrete aggregate on properties of cement mortar. Constr Build Mater 98: 1-7. https://doi.org/10.1016/j.conbuildmat.2015.08.087
[16] Xuan DX, Zhan BJ, Poon CS (2016) Assessment of mechanical properties of concrete incorporating carbonated recycled concrete aggregates. Cement Concr. Compos. 65: 67-74. https://doi.org/10.1016/j.cemconcomp.2015.10.018
[17] Zha X, Yu M, Ye JQ, Feng GL (2015) Numerical modeling of supercritical carbonation process in cement-based materials. Cement Concrete Res 72: 10-20. https://doi.org/10.1016/j.cemconres.2015.02.017
[18] Jang JG, Lee HK (2016) Microstructural densification and CO_2 uptake promoted by the carbonation curing of belite-rich Portland cement. Cement Concrete Res 82: 50-57. https://doi.org/10.1016/j.cemconres.2016.01.001
[19] Hover KC (2011) The influence of water on the performance of concrete. Constr Build Mater 25(7): 3003-3013. https://doi.org/10.1016/j.conbuildmat.2011.01.010
[20] Balabanić G, Bićanić N, Đureković A (1996) The influence of w/c ratio, concrete cover thickness and degree of water saturation on the corrosion rate of reinforcing steel in concrete. Cement Concrete Res 26(5): 761-769. https://doi.org/10.1016/S0008-8846(96)85013-7
[21] Zhang S, Yuan Q, Ni J, Zheng KR, Xu YQ, Zhang JL (2024) CO_2 utilization and sequestration in ready-mix concrete — a review. Science of the Total Environment 907: 168025. https://doi.org/10.1016/j.scitotenv.2023.168025
[22] Yang YH, Xu G, Tian B (2021) Carbonation characteristics of cement-based materials under the uniform distribution of pore water. Constr Build Mater 775: 121450. https://doi.org/10.1016/j.conbuildmat.2020.121450
[23] Von Greve-Dierfeld S, Lothenbach B, Vollpracht A, et al (2020) Understanding the carbonation of concrete with supplementary cementitious materials: a critical review by RILEM TC 281-CCC. Materials and Structures 53(6): 136. https://doi.org/10.1617/s11527-020-01558-w
[24] Elsalamawy M, Mohamed AR, Kamal EM (2019) The role of relative humidity and cement type on carbonation resistance of concrete. Alexandria Engineering Journal 58(4): 1257-1264. https://doi.org/10.1016/j.aej.2019.10.008
[25] Chen Y, Liu P, Yu (2018) Effects of environmental factors on concrete carbonation depth and compressive strength. Mater. 11(11): 2167. https://doi.org/10.3390/ma11112167
[26] Anwar M, Emarah DA (2022) Durability of Blast-Furnace Slag Cement Concrete with Different Curing Methods. Journal of Engineering Sciences 50(5): 276-291. https://doi.org/10.21608/jesaun.2022.140887.1142
[27] Mehdizadeh H, Jia X, Mo KH, Ling TC (2021) Effect of water-to-cement ratio induced hydration on the accelerated carbonation of cement pastes. Environmental Pollution 280: 116914. https://doi.org/10.1016/j.envpol.2021.116914
[28] Yang QT, Liu M, Li JX, Chen X (2024) Study on the degradation models based on the experiments considering the coupling effect of freeze-thaw and carbonation. Structures 64: 106659. https://doi.org/10.1016/j.istruc.2024.106659
[29] Puertas F, Palacios M, Vázquez T (2006) Carbonation process of alkali-activated slag mortars. Journal of materials science 41(10): 3071-3082. https://doi.org/10.1007/s10853-005-1821-2

[30] Gu YZ, Wang XD, Xu ZB, Wei SZ, Yuan QX, Zhang YS (2024) Effect of supercritical CO_2 carbonation parameters on heavy metal solidification and environmental stability of coal fly ash. Journal of Material Cycles and Waste Management 26(5): 3047-3058. https://doi.org/10.1007/s10163-024-02027-0

[31] Samarakoon MH, Ranjith PG, Xiao F, Isaka BL, Gajanayake SM (2021) Carbonation-induced properties of alkali-activated cement exposed to saturated and supercritical CO_2. International Journal of Greenhouse Gas Control 110: 103429. https://doi.org/10.1016/j.ijggc.2021.103429

[32] Bao H, Yu M, Chi Y, Liu Y, Ye JQ (2021) Performance evaluation of steel-polypropylene hybrid fiber reinforced concrete under supercritical carbonation. J. Build. Eng. 43: 103159. https://doi.org/10.1016/j.jobe.2021.103159

[33] Yuan QX, Yang G, Zhang YS, Wang T, Wang JW, Romero CE (2022) Supercritical CO_2 coupled with mechanical force to enhance carbonation of fly ash and heavy metal solidification. Fuel 315: 123154. https://doi.org/10.1016/j.fuel.2022.123154

[34] Liu C, Wang J, Yu C, Kong Y, Hu Z, Liu J (2024) Carbonation strengthening mechanism of dry cement-based materials under supercritical carbon dioxide, J. Build. Eng. 94: 109915. https://doi.org/10.1016/j.jobe.2024.109915

[35] Bao H, Xu G, Yu M, Wang Q, Li RD, Saafi M, Ye J (2022) Evolution of ITZ and its effect on the carbonation depth of concrete under supercritical CO_2 condition. Cement Concr. Compos. 126: 104336. https://doi.org/10.1016/j.cemconcomp.2021.104336

[36] Zha X, Ning J, Saafi M, Dong L, Dassekpo JM, Ye JQ (2019) Effect of supercritical carbonation on the strength and heavy metal retention of cement-solidified fly ash. Cement Concrete Res 120: 36-45. https://doi.org/10.1016/j.cemconres.2019.03.005

[37] Farahi E, Purnell P, Short N (2013) Supercritical carbonation of calcareous composites: influence of curing. Cement Concr. Compos. 43: 48-53. https://doi.org/10.1016/j.cemconcomp.2013.06.008

[38] Dong S, Xing T, Zhao L, Zhu C, Yao X, Zhao S, Teng H (2023) Physical and chemical effects of H_2O on mineral carbonation reactions in supercritical CO_2. Applied Geochemistry 155: 105668. https://doi.org/10.1016/j.apgeochem.2023.105668

[39] Kim J, Azimi G (2021) The CO_2 sequestration by supercritical carbonation of electric arc furnace slag. Journal of CO_2 Utilization 52: 101667. https://doi.org/10.1016/j.jcou.2021.101667

[40] Han DR, Namkung H, Lee HM, Huh DG, Kim HT (2015) CO_2 sequestration by aqueous mineral carbonation of limestone in a supercritical reactor. Journal of Industrial and Engineering Chemistry 21: 792-796. https://doi.org/10.1016/j.jiec.2014.04.014

[41] Bao H, Zheng Z, Xu G, Li R, Wang Q, Saafi M, Ye Y (2024) Performance and mechanism of sand stabilization via microbial-induced $CaCO_3$ precipitation using phosphogypsum. Journal of Cleaner Production 468: 142999. https://doi.org/10.1016/j.jclepro.2024.142999

[42] Jiang Q, Yu C, Zhou M (2023) Effect of typical formworks and release agents on aesthetical surface quality of concrete. Magazine of Concrete Research 75(24): 1285-1296. https://doi.org/10.1680/jmacr.23.00063

[43] Savukaitis G, Daukys M, Juoinas S, Grinys A, Kriptaviius D (2021) The influence of new and used formwork coated with different release agents on the appearance of the formed concrete surface. J. Build. Eng. 42: 102807. https://doi.org/10.1016/j.jobe.2021.102807

[44] Tang S, Huang J, Duan L, Yu P, Chen E (2020) A review on fractal footprint of cement-based materials. Powder technology 370: 237-250. https://doi.org/10.1016/j.powtec.2020.05.065

[45] Papadakis VG, Vayenas CG, Fardis MN (1991) Fundamental modeling and experimental investigation of concrete carbonation. ACI Mater. J. 88 (4): 363-373. https://doi.org/10.14359/1863

[46] McPolin DO, Basheer PA, Long AE, Grattan KT, Sun T (2007) New test method to obtain pH profiles due to carbonation of concretes containing supplementary cementitious material. J. of Mater. in Civil Engineering 19(11): 936-946. https://doi.org/10.1061/(ASCE)0899-1561(2007)19:11(936)
[47] Saetta AV, Schrefler BA, Vitaliani RV (1995) 2-D model for carbonation and moisture/heat flow in porous materials. Cement Concrete Res 25(8): 1703-1712. https://doi.org/10.1016/0008-8846(95)00166-2
[48] Zha X, Ning J, Saafi M, Dong L (2019) Effect of supercritical carbonation on the strength and heavy metal retention of cement-solidified fly ash. Cem. Concr. Res. 120: 36-45. https://doi.org/10.1016/j.cemconres.2019.03.005
[49] GB/T 50082-2009, Standard for Long-term Performance and Durability Test Methods for Ordinary Concrete. 2009-11-30. (in Chinese)
[50] Baroghel-Bouny V (2007) Water vapour sorption experiments on hardened cementitious materials. Part II: Essential tool for assessment of transport properties and for durability prediction. Cement Concrete Res 37(3): 438-454. https://doi.org/10.1016/j.cemconres.2006.11.019
[51] Jamil S, Shi J, Idrees M (2023) Effect of various parameters on carbonation treatment of recycled concrete aggregate using the design of experiment method. Constr Build Mater, 382: 131339. https://doi.org/10.1016/j.conbuildmat.2023.131339
[52] A practical guide to microstructural analysis of cementitious materials. Boca Raton, FL, USA: Crc Press (2016).
[53] De Weerdt K, Plusquellec G, Revert AB, Geiker MR, Lothenbach B (2019) Effect of carbonation on the pore solution of mortar. Cement Concrete Res, 118: 38-56. https://doi.org/10.1016/j.cemconres.2019.02.004
[54] Zhu J, Zhu G, Qi F, Li H, Chen Y, Li S, Guo Y (2024) Research Progress on Preparation and Comprehensive Utilization of Solid Waste-Based Calcium Silicate Hydrates. Silicate Bulletin 43(02): 517-533. (in Chinese)
[55] Li X, Fan Y, Wu C, Wang L (2024) Advances in Molecular Dynamics-Based Characterization of Water and Ion Adsorption and Transport in CSH Gels. Polymers 16(23): 3285. https://doi.org/10.3390/polym16233285
[56] Aretxabaleta XM, López-Zorrilla J, Etxebarria I, Manzano H (2023) Multi-step nucleation pathway of CSH during cement hydration from atomistic simulations. Nature Communications 14(1): 7979. https://doi.org/10.1038/s41467-023-43500-y
[57] Cuesta A, Santacruz I, Torre AG, Dapiaggi M, Zea-Garcia JD, Aranda MA (2021) Local structure and Ca/Si ratio in CSH gels from hydration of blends of tricalcium silicate and silica fume. Cement Concrete Res 143: 106405. https://doi.org/10.1016/j.cemconres.2021.106405
[58] Min Q, Ku T, He B, Wei R, Liu C, Zhang L, Liu L (2024) Effect of Carbide Slag Addition on Properties and Carbon Sequestration Efficiency of Fresh Cement Slurry Mixed with CO_2. Mater. Herald 38(23): 102-107. (in Chinese)
[59] Ngo I, Ma L, Zhai J, Wang Y (2023) Enhancing fly ash utilization in back-fill materials treated with CO_2 carbonation under ambient condi-tions. International Journal of Mining Science and Technology 33(3): 323−337. https://doi.org/10.1016/j.ijmst.2023.02.001
[60] Fu X, Guerini A, Zampini D, Rotta Loria AF (2024) Storing CO_2 while strengthening concrete by carbonating its cement in suspension. Communications Materials 5(1): 109. https://doi.org/10.1038/s43246-024-00546-9
[61] Yuan Z, Xu-peng TA, Shu-bing Q, You-min H (2023) Analysis of Carbon Storage Potential of CO_2

Foamed Concrete. Environmental Science 44(9): 5308-5315. https://doi.org/10.13227/j.hjkx.202210180

[62] Qian R, Lin WW, Yang C, Zhao R, Ye Z, Kong D, Zhang Y (2024) Investigations on carbon-sequestration optimization of recycled coarse-aggregate and its effects on concrete performances. J. Build. Eng. 90: 109453. https://doi.org/10.1016/j.jobe.2024.109453

[63] Shen J, Dangla P, Thiery M (2013) Reactive transport modeling of CO_2 through cementitious materials under CO_2 geological storage conditions. International Journal of Greenhouse Gas Control 18: 75-87. https://doi.org/10.1016/j.ijggc.2013.07.003